J Mater Sci (2022) 57:2318–2333

Polymers & biopolymers

The impact of eco-friendly chemical incorporation on the thermal oxidation process of flax fiber prior to carbonization and activation

Md. Mahbubor Rahman[1,2] and Ismail Karacan[1,*]

[1] Department of Textile Engineering, Erciyes University, 38280 Kayseri, Turkey
[2] Bangladesh University of Textiles, Tejgaon, Dhaka 1208, Bangladesh

Received: 1 October 2021
Accepted: 29 October 2021
Published online: 3 January 2022

ABSTRACT

The oxidative thermal stability of plant-based microcrystalline flax fiber was developed by incorporating diammonium phosphate (DAP), boric acid, and urea (in brief DAP-BAU) followed by a multistep thermal oxidation process. By utilizing a set of measurements, including X-ray diffraction, differential scanning calorimetry (DSC), thermogravimetric analysis (TGA), and infrared (IR) spectroscopy analysis, the impact of DAP-BAU inclusion on the thermal stability of flax fibers was studied. The findings of IR spectra and X-ray diffraction analysis revealed that the dehydrogenation and dehydration processes cause a progressive and steady loss of inter- and intramolecular H-bondings. Infrared spectra also showed the development of C = C double bonds associated with the crosslinked ladder structure formation. DSC and TGA findings revealed that DAP-BAU incorporation boosted thermal stability by generating ladder-like structure formation and restricted the development of volatile by-products by inhibiting the fundamental hydroxyl groups with increasing oxidation time. The overall findings of this study confirm that DAP-BAU incorporated and 125 min stabilized (at 245 °C) flax fibers attain complete thermal stability and are ready for utilizing in the subsequent carbonization and activation stages in activated carbon fiber manufacturing.

Introduction

Activated carbon is a nontoxic and reusable carbon material that contains different surface functional groups having attraction toward various adsorbates, validating the great usage of them in the industrial effluent treatment. There are four types of activated carbon: activated carbon fiber (ACFs), granular activated carbon, powdered activated carbon, and activated carbon pellet. Of these four types, ACFs have

Handling Editor: Stephen Eichhorn.

Address correspondence to E-mail: ismailkaracanxxx@gmail.com

https://doi.org/10.1007/s10853-021-06686-4

the benefit of being formed fibrously from fibers; it is simpler to create entanglement with each other creating web and no post-treatment need [1–5]. ACFs have a higher specific surface area and large pore volume and are widely used in catalysis [6], purification [7], separation [8], and energy storage [9]. As the cost of manufacturing of the synthetic precursor is expensive and the interest in activated carbon fibers rises, inexpensive natural resources need to be sought for the production of ACFs [10, 11]. The natural precursor materials, including sisal [12], viscose rayon [13], hemp [10], paper [14], wood [15, 16], coconut shell [17], and cotton stalk [18], were mentioned to use in activated carbon fiber manufacturing. Nonetheless, aside from activated carbon, there are very few published articles of flax being used as a raw material for producing ACFs [19, 20].

Flax fiber (*Linum usitatissimum L.*) is one of the strongest natural bast fibers that contain cellulose (70.5%), hemicellulose (16.5%), lignin (2.5%), and pectin (0.9%). The structure of flax fibers is highly complex, and it could be compared with a composite structure. Flax fibers are made up of a number of polyhedron-shaped primary fibers that are overlapped across a wide area and kept together by an interphase made up mostly of pectin and hemicellulose [21]. Cellulose, one of the main constituents of flax fiber, is a promising precursor element of carbon and activated carbon fiber manufacturing. The cellulose has a well-ordered crystal structure, and it goes through thermal decomposition without melting. The hydroxyl groups in the cellulose structure rapidly generate intra- and intermolecular hydrogen H-bonds in the thermal stabilization process, resulting in a variety of structured crystalline configurations [22]. Cellulose was reported to be used alone [22–24] and also with lignin [25, 26] in the published literature for this purpose. Lignin, another component of flax fiber, is a natural high molecular weight amorphous polyaromatic macromolecule made up of phenyl propane entities with methoxyl, hydroxyl, and carbonyl substitutions [27]. Lignin has higher carbon content, around $60-65\%$ indicating a higher carbon yield in manufactured carbon and activated carbon fiber [25]. Lignin was mentioned to be employed alone for this purpose in the published literature [27–30].

DAP and boric acid were used to impregnate with flax fibers as flame retardation agents in this study. DAP, boric acid, and urea are less expensive and environmentally friendly chemicals. During the oxidation reactions, the formation of boron phosphate occurs in the presence of urea on the hydroxyl groups of cellulose, hemicellulose, and lignin components of flax fibers [31–33]. DAP and boric acid react and form boron phosphate, ammonia, and water as follows [34].

$$(NH_4)_2HPO_4 + H_3BO_3 \rightarrow BPO_4 + 2NH_3 + H_2O$$

Urea is reported to be a swelling agent and contains strong hydrogen bonding groups for cellulosic fibers. The generally accepted view is that urea melts at around 140 °C and is fluid between 140 and 160 °C. Urea is also known to penetrate and create buffering action to prevent the degradation of cellulosic structures [32]. As a result of DAP and boric acid decomposition, dehydration and preliminary carbonization reactions are expected during the oxidation reactions of flax fibers. The chemical reaction between hydroxyl groups of cellulose, hemicellulose, and lignin is expected to prevent the formation of tarry (i.e., levoglucosan) substances during the oxidation reactions [35].

The objective of the current study was to explore the influence of DAP-BAU pretreatment on the thermal oxidation of flax fibers at temperatures up to 245 °C for different stabilization durations. Thermal and structural properties were characterized by means of DSC, TGA, FT-IR, and XRD to observe and follow the alterations that took place in the oxidation process of the DAP-BAU incorporated and oxidized flax samples.

Experimental details

Thermally stabilized sample preparation

To remove surface contaminants from the fibers, the raw flax yarns were mercerized for 60 min at room temperature in an 18% NaOH aqueous solution. After removing surface contaminants, the sample was dried in the air for 4 h at 80 °C after being allowed to dry overnight at 25 °C (Fig. 1).

The flax yarns were treated in a water solution containing 3% diammonium phosphate or DAP ($(NH_4)_2HPO_4$), 3% boric acid (H_3BO_3), and 3% urea ($NH_2–CO–NH_2$) for 6 h at room temperature. The pH value of the solution was 7.05 at 26.1 °C. The flax specimens were dried at 70 °C for 5 h after

Figure 1 Chemical impregnated flax fiber samples.

performing chemical integration. For the oxidation process, a multistep approach was utilized at temperatures 160, 180, 200, 220, and 245 °C. Oxidation durations were 25, 50, 75, 100, and 125 min, which were employed in different stabilization stages individually.

Experimental data collection

Differential scanning calorimetry (DSC) analysis

A PerkinElmer Diamond DSC apparatus was used to conduct differential scanning calorimetry (DSC) measurements. The sample weights utilized were typically about 5 mg. A heating rate of 10 °C/min was specified, with a maximum temperature range of 450 °C. For heat flow assessment, indium (m.p. 156.6 °C and $\Delta H = 28.45$ J/g) was employed. Temperature calibration was performed with indium and zinc (m.p. 419.51 °C) standards. The samples were examined at a flow rate of 50 mL/min of nitrogen [36].

Thermogravimetric (TGA) analysis

The TGA profiles of the pristine and oxidized samples were assembled utilizing a PerkinElmer TGA analyzer. The uppermost temperature was kept 1000 °C, and the heating rate was 10 °C/min with a sample weight of 5–6 mg. The nitrogen gas flow rate was kept at 200 ml/min during the experiment. The adjustment of TGA temperature was set employing the standard melting points of tin, aluminum, zinc, indium, and gold [37, 38].

Fourier transform infrared (IR) analysis

Infrared spectroscopy analysis was executed by a PerkinElmer® FT-IR spectrometer in absorbance mode. The mean value was taken of 50 interferograms by utilizing a Norton–Beer apodization algorithm. Every specimen band was ratioed by keeping fixed system adjustments compared to a compatible amount of background scans. By employing the SPECTRUM program and the curve-fitting technique, all of the characteristic bands were examined [37, 38].

X-ray diffraction (XRD) analysis

A Bruker® AXS D8 X-ray diffractometer was used in attaining X-ray diffraction profiles of the flax fiber samples. In the 10–40° 2θ scattering range, X-ray diffraction traces of the pristine and oxidized flax fibers were attained. Lorentz and polarization corrections were performed additionally in achieving X-ray diffraction profiles [39].

Data analysis

X-ray data curve-fitting

For dissociating the overlapped peaks, all the obtained X-ray diffraction traces were attuned employing a curve-fitting method defined by Hindeleh et al. [39]. The Gaussian and Cauchy functions were considered for each profile. In the curve-fitting strategy, computer programming provides specific peak parameters such as peak height in electron unit, peak position (2θ), peak width at half height, and profile function (f).

Apparent X-ray crystallinity

Apparent X-ray crystallinity (χ_c) is the integrated intensity ratio of the values beneath the resolved peaks to the values of the cumulative scatter beneath the observational peak [40]. Mostly, this is presented as in Eq. 1. The investigation was accomplished between 5° and 35°, in 2θ range.

$$\chi_c = \frac{\int_0^{\infty} I_{cr}(2\theta)d(2\theta)}{\int_0^{\infty} I_{tot}(2\theta)d(2\theta)} \quad (1)$$

X-ray oxidation index

In evaluating the X-ray oxidation index, Eq. 2 [41] was employed in this investigation.

$$\text{X - ray oxidation index } (\%) = \frac{I_0 - I}{I_0} \times 100\% \quad (2)$$

where I_o represents the (002) peak intensity (at 2θ = 22.4°) of the pristine flax sample, while I represents the (002) peak intensity (at 2θ = 22.4°) of oxidized flax sample. By employing the curve-fitting strategy, the intensity values were attained.

Apparent lateral crystallite size

By employing Stoke's deconvolution approach, the peak widths at half height were attuned [42]. For the particular reflection of oxidized flax samples, the apparent lateral crystallite size was evaluated employing Scherrer Eq. 3.

$$L_{(hkl)} = \frac{K\lambda}{\beta.\cos(\theta)} \quad (3)$$

where $L_{(hkl)}$ represents the mean crystallite length upright to the hkl planes, λ represents the radiation wavelength (λ = 0.15406 nm), K represents a Scherrer parameter, β represents breadth at half-maximum intensity, and θ represents the Bragg angle of the concerning reflection.

Results and discussion

Differential scanning calorimetry (DSC)

DSC thermograms were utilized to investigate the structural changes occurring in the oxidation reactions of flax fibers impregnated with DAP-BAU for different oxidation durations. The DSC profile of raw flax fiber illustrated in Fig. 2a represents a wide endotherm immediate 100 °C due to the presence of water vapor. A wider and stronger endotherm between 340 and 370 °C, having a peak temperature of 360 °C, ascribed to depolymerization and decomposition reactions of cellulose and hemicellulose following the reactions resulting in the development of levoglucosan and its decomposition constituents [43]. The intensity of this peak weakened and broadened in intensity with growing oxidation times. The DSC thermogram of raw flax fiber also showed an extra peak as a wide exotherm between 350 and 400 °C, having 373 °C peak temperature owing to the oxidation of levoglucosan-based volatile pyrolysis compounds [44]. DAP-BAU pretreatment and thermal stabilization in the air atmosphere seemed to show a major impact on the DSC profiles of oxidized flax fibers. Figure 2b–f represents the DSC traces of DAP-BAU integrated flax fibers oxidized for 25 to 125 min oxidation durations.

The DSC profiles of the sample oxidized for 50 min at 245 °C shifted to 255 °C owing to the depolymerization reactions of remaining cellulose and hemicellulose. The decomposition temperature of the flax fiber oxidized for 50 min is 105 °C, which is lesser than the raw flax fiber. As a potent fire retardant, DAP-BAU resulted in a severe depletion of the decomposition temperature of cellulose [31]. Decomposition temperature reduction attributes to the catalyzed dehydration reactions of cellulosic

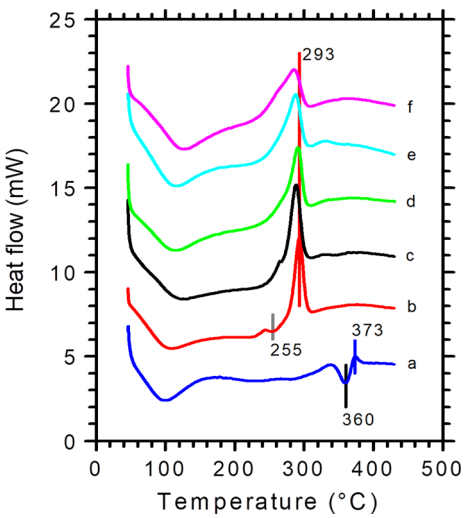

Figure 2 DSC profiles of raw **a** and DAP-BAU pretreated-oxidized flax fibers for variable oxidation durations. **b** 25 min; **c** 50 min; **d** 75 min; **e** 100 min; **f** 125 min.

structural units by the chemical processes occurring within the hydroxyl groups of cellulose, hemicellulose, lignin, and DAP-BAU. The substantial decrease of cellulose–hemicellulose–lignin decomposition temperature after the DAP-BAU treatment is also thought to be due to the drop of the degree of crystallinity with escalating oxidation time [45].

The extent below the central endothermic peak is noticed to be dropped after the oxidation time of 25 min and disappeared completely between 50 and 125 min, respectively; this behavior is accredited to the dehydration process that occurred by the chemical reactions occurring in the core hydroxyl groups of cellulose (–CH_2–OH) rings, hemicellulose, and lignin. This process is estimated to cause the removal of –OH groups from cellulose, hemicellulose, and lignin chains and in the loss of H-bonds from the –OH groups in producing water. The development of double-bonded groups, typically C = O and C = C, also takes place. Due to the dehydration process, the structure of cellulose–hemicellulose–lignin is sustained, the development of volatile derivatives is prohibited, and the weight loss is typically restricted to water loss alone. [22].

After 50 min of oxidation at 245 °C, the region associated with the decomposition endotherm is decreased and then eliminated (Table 1). DAP-BAU pretreatment limits the depolymerization processes and prevents the synthesis of levoglucosan, which results in the diminution and final removal of the endotherm. This outcome is thought due to the higher carbon yield in the samples generated for DAP-BAU pretreatment and increased oxidation times. The vanishing of the decomposition endotherm for 50 min oxidation time and beyond also shows the formation of high temperature-resistant and thermally stabilized structural units. The DSC traces of the 50 min and above-timed oxidized samples also represented the complete vanishing of the decomposition endotherms originated from the cellulose I–hemicellulose–lignin structure loss and the development of thermally stabilized and crosslinked structural units.

The DSC traces of DAP-BAU treated flax fibers stabilized at 245 °C for oxidation times of 25 min and beyond showed a strong intensity exotherm at around 286–293 °C. This exotherm kept its presence at the oxidation times between 25 and 125 min (Fig. 2 and Table 1) and is accredited to the crosslinking process of cellulose–hemicellulose–lignin rings occurring in the decomposition and dehydration reactions. The exothermic heat below this peak did keep its presence but gradually lessened in intensity at the oxidation times between 25 and 125 min, while the entire cellulose structure was fully converted into greatly cyclized and crosslinked groups of chains.

Thermal analysis (TGA)

The TGA method continuously measures the weight loss of samples as a function of time or temperature at a linear rate. Various steps in the TGA analysis provide important information on thermal stability, original sample composition, the thermal stability of intermediates formed, and kinetic data. Essentially, the TGA method is dynamic in nature and offers quantitative information about the thermal stability of the samples under investigation. Thermal analysis is one of the most important techniques to observe and analyze the thermal behavior of samples under investigation. In the present investigation, the TGA method has been employed to investigate the thermal behavior of flax fibers. The weight loss occurring during TGA scanning of flax fibers is attributed to the

Table 1 Thermal properties of raw and oxidized flax fibers pretreated in DAP-BAU

Oxidation time (min)	Decomposition temperature (°C)	Area of (ΔH) decomposition (J/g)a	Carbon formation exotherm (°C)	Area of carbon formation exotherm (J/g)	Exotherm due to levoglucosan oxidation (°C)
0	360	24.739	–	–	373
25	255	6.322	293	−67.267	–
50	–	–	288	−81.579	–
75	–	–	290	−81.055	–
100	–	–	288	−71.046	–
125	–	–	286	−68.659	–

decomposition of cellulose, hemicellulose, and lignin structural components. Usually, higher decomposition temperatures result in higher thermal stability [46].

In cellulosic fibers, there is no glass transition or melting transitions. The only transition is that of decomposition around 340–380 °C at a heating rate of 10 °C/min. It should be emphasized that the exact positions of these transitions heavily depend on the rate of heating and the impurities present in the material. According to the published literature [47], the heating rate is an important factor for differentiating the relative characteristics of fibers. It seems that when the heating rates increased from 5 to 150 °C/min, decomposition maxima increased from 321 to 394 °C for water-retted lignocellulosic flax fibers [47].

Thermogravimetric analysis was utilized for characterizing the thermal stability of pristine and DAP-BAU incorporated and oxidized flax fibers. An initial evaluation of the pyrolysis processes can be carried out based on comparative decomposition temperatures and dTGA curve patterns. Comparatively higher and steeper peaks indicate quicker reactions, and greater weight loss results in lower carbon yield. On the other hand, broader pyrolytic peaks result in rational reactions and therefore generate higher carbon yield. For flax-based activated carbon fiber production, faster pyrolysis (such as carbonization) in the inert environment is unfavorable. It is expected to accelerate side reactions, resulting in lower-carbon yields and the constituents having volatile carbon [13]. Large quantities of organic acids, aldehydes, and carbon dioxide are released as volatile derivatives during faster pyrolysis leading to poor carbon yields. The oxygen-containing air environment is also essential in obtaining higher carbon yields. Under an inert atmosphere, the thermal decomposition of flax fibers shows a single-step decomposition which results in one dTGA curve. This decomposition pattern is attributed to the combination of the main structural components of hemicellulose, cellulose, and lignin in flax fibers. According to Thuault et al. [48], the following transition temperatures were observed in a typical TGA scan of flax fiber; hemicellulose at 250–320 °C, cellulose at 340–400 °C, and lignin at 400–470 °C.

Carbon yield and weight loss could be used in comparing the relative yield values of the carbonization stage for variable oxidation times. The TGA profiles of pristine and DAP-BAU incorporated flax fibers oxidized in the air for oxidation times of 0 and 125 min are illustrated in Fig. 3. All the TGA curves show weight loss at about 50–120 °C indicating the presence of water on the surface of the samples. The TGA profile of pristine flax fiber indicated that the weight loss occurs in a small temperature range of 250 to 400 °C. The thermal decomposition process of pristine flax fibers was initiated at 250 °C and sustained until 400 °C (Fig. 3a).

Faster weight loss occurring in the range of 250 to 400 °C in the inert environment indicates the occurrence of higher thermal decomposition. The highest weight loss was observed at 355 °C, the carbon yield value was 42.5% at 1000 °C. In contrast, the TGA profiles of DAP-BAU incorporated and oxidized flax fibers demonstrated a reduced weight loss ratio with growing oxidation time, signifying escalating carbon yield due to the greater crosslinking and aromatization reactions among the flax cellulose–hemicellulose–lignin chains. The TGA curves of the DAP-BAU incorporated-oxidized flax fibers exhibited slower weight loss at temperatures between 250 and 500 °C owing to aromatization and crosslinking processes.

The carbon yield (%) at 500 and 1000 °C temperatures attained from the original and DAP-BAU incorporated flax fibers for variable oxidation times are presented in Fig. 4. The outcomes indicated a steady growth of carbon yield for higher oxidation times. Carbon yield ratios are higher at 500 °C than

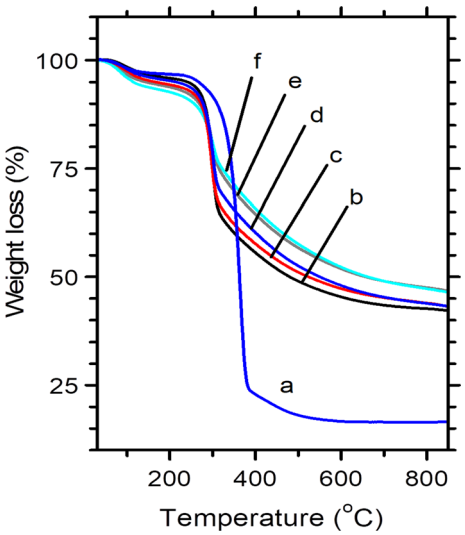

Figure 3 TGA thermograms of raw **a** and DAP-BAU pretreated-oxidized flax fibers for variable oxidation durations. **b** 25 min; **c** 50 min; **d** 75 min; **e** 100 min; **f** 125 min.

those at the temperature of 1000 °C growing from 49 to 58%. The carbon yield ratio increased to a maximum value of 42.5% at 1000 °C for the DAP-BAU incorporated and 125 min oxidized flax fibers.

dTGA curves of TGA thermograms are presented in Fig. 5. The dTGA curve of the original flax fibers (Fig. 5a) exhibits two exothermic peaks. The peak appearing as a broad shoulder centered around 290 °C is assigned to the decomposition of hemicellulose, and a well-defined peak centered around 365 °C is attributed to the decomposition of cellulose. Lignin decomposition peak did not appear in the dTGA thermograms. Following the oxidation reactions, the dTGA peak for the oxidized samples shifts from 365 °C due to the decomposition of cellulose to 300 °C. Hemicellulose decomposition peak was located at 290 °C but disappeared in the oxidized samples. Lignin decomposition peak was not detected in the samples, possibly due to its lower existence.

FT-IR spectroscopy analysis

In the present investigation, infrared spectroscopy was extensively utilized to investigate structural changes occurring during the oxidation reactions. Structural changes happening during the oxidation process were monitored and followed as a function of oxidation time. Information from infrared spectroscopy is one of the most useful and fundamental approaches for the understanding of the structure of cellulose, hemicellulose, and lignin, mainly for identifying the network of hydrogen bonds in the molecular structure of flax fibers. The infrared bands of pristine and oxidized flax fibers are presented in Fig. 6 for different oxidation times between 4000 and 2000 cm^{-1} region.

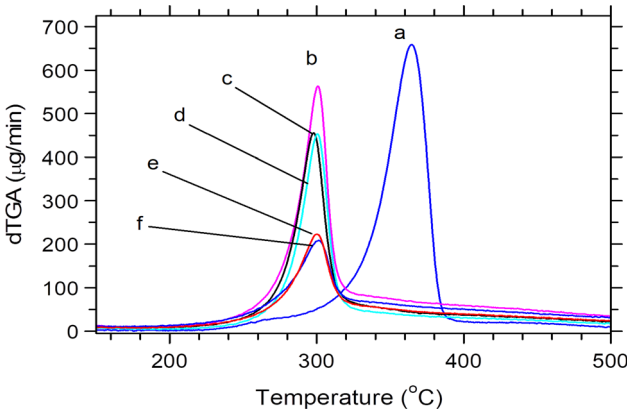

Figure 5 dTGA thermograms of raw **a** and DAP-BAU pretreated-oxidized flax fibers for variable oxidation durations. **b** 25 min; **c** 50 min; **d** 75 min; **e** 100 min; **f** 125 min.

The IR range 4000 to 3000 cm^{-1} is considered to be due to intramolecular and intermolecular H-bonded OH group bands. The OH groups available in the molecular structure of cellulose, hemicellulose, and lignin readily form intra- and intermolecular hydrogen bonds, which results in the formation of crystalline regions [22, 45, 49]. In the infrared spectrum of cellulose, the 3000–2000 cm^{-1} region is assigned to the methine (C-H) and methylene (CH_2) stretching bands. The IR spectrum of pristine flax fiber contains vibrations due to cellulose, hemicellulose, and lignin components [50]. Band assignments for the 4000–500 cm^{-1} region of the IR spectrum of flax fiber are listed in Table 2. Following DAP-BAU pretreatment and oxidation in an air atmosphere, noticeable

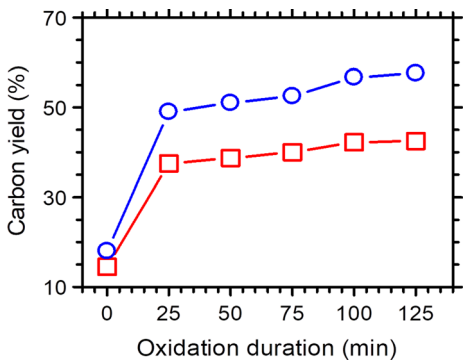

Figure 4 Variation of carbon yields at scanning temperatures 500 °C (O) and 1000 °C (□) of the raw and oxidized flax fibers.

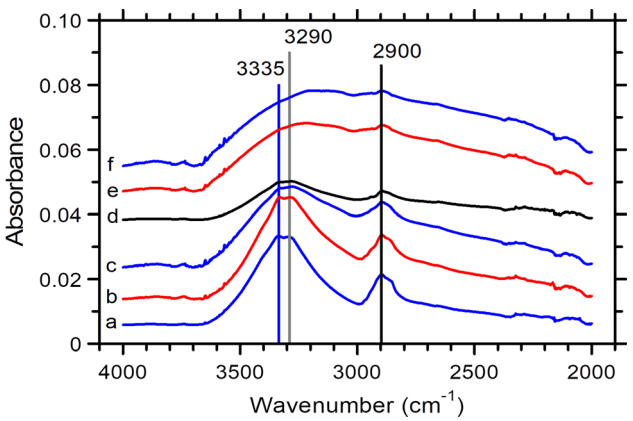

Figure 6 IR spectra in the range 4000–2000 cm^{-1} of raw **a** and DAP-BAU pretreated-oxidized flax fibers for variable oxidation durations. **b** 25 min; **c** 50 min; **d** 75 min; **e** 100 min; **f** 125 min.

deviations in comparative intensity values were observed as H-bonding and CH stretching vibrations in the area spanning 4000 to 3000 cm^{-1}.

The IR spectrum of original flax fiber covering 3700 and 3000 cm^{-1} regions illustrated in Fig. 7 was analyzed and fitted with nine peaks using a peak separation procedure. Peak separation procedure was performed using band positions located at 3540, 3480, 3435, 3380, 3340, 3290, 3235, 3175, and 3105 cm^{-1}. The infrared peak located at 3540 cm^{-1} is attributed to free OH vibrations. On the other hand, the IR bands located at 3540, 3480, 3435, 3380, and 3340 cm^{-1} are attributed to the OH vibration of the intramolecular H-bonds (Table 2).

Intermolecular H-bonded bands are positioned at 3290, 3235, 3175, and 3105 cm^{-1}, respectively. It seems that intermolecular H-bonding shows a higher delicacy to temperature fluctuations than intramolecular H-bonding [57]. OH, CH, and CH_2 bands positioned in the range from 3700 to 3000 cm^{-1} progressively lost intensities yet never vanished entirely. OH spectra attributed to oxidized flax fibers primarily exposed broadening but lost maximum

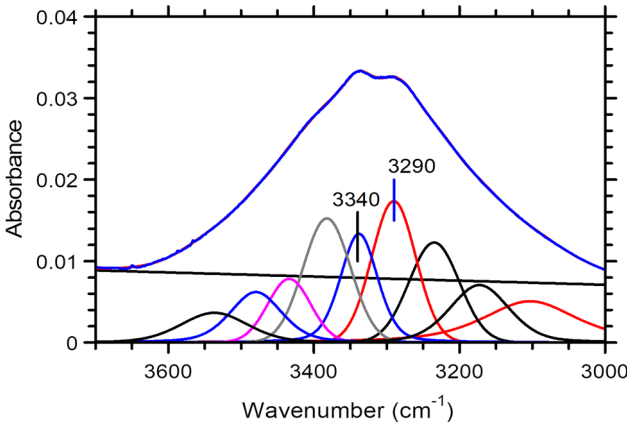

Figure 7 Curve-fitting of the infrared spectrum of pristine flax fibers in the 3700–3000 cm^{-1} region.

Table 2 Band assignments for the 4000–500 cm^{-1} region of the infrared spectrum of flax fiber

Wavenumber (cm^{-1})	Assignment [51–56]
3540	Free OH vibrations
3540, 3480, 3435, 3340, 3290, 3235, 3105	OH stretching intermolecular hydrogen bonding
2922	CH_2 asymmetrical stretching
2900	CH and CH_2 stretching
2870	CH and CH_2 symmetrical stretching
1730	C = O stretch (before oxidation), hemicellulose
1715	C = O stretch in unconjugated ketones, carbonyls, and ester groups of hemicellulose structure (after oxidation)
1635	adsorbed H_2O
1610	C = C stretching, aromatic skeletal mode (lignin)
1455	CH-deformation and CH_2 bending
1430	CH_2 and O–C–H in-plane bending, crystalline cellulose
1370	CH_2 bending (the crystalline phase from cellulose)
1317	CH_2 wagging
1235	C–O stretching in acetyl group
1205	OH in-plane bending
1155	C–O–C asymmetrical stretching of cellulose and hemicellulose (crystalline phase mainly from cellulose); A decrease in the intensity of this vibration is attributed to a decrease in the degree of crystallinity
1102	Asymmetrical in-phase ring stretching of cellulose (crystalline)
1054	C–O bond stretching and C–O deformation
1030	CO stretching
1007	C–O stretching
895	Cellulose-based asymmetrical out of phase ring stretching (C–O–C)
800	Cellulose-based ring breathing mode
663	OH, out of plane bending

intensity for higher oxidation time. The dehydration process resulted from the interaction of hydroxyl and boron phosphate (BPO_4) groups in the initial steps of oxidation reactions, the intensities of the vibrations located at 3290, 3235, 3175, and 3105 cm^{-1} involved in the intermolecular H-bonding and the OH groups gradually weakened with increasing oxidation time. This behavior indicated an interruption in intermolecular H-bonding. The IR spectra located at 3520, 3450, 3405, and 3350 cm^{-1} attributed to the intramolecular H-bonded OH groups also lost their intensity yet never vanished entirely. This outcome suggests that maximum oxidation reactions occurred within OH-groups of cellulose, hemicellulose, and lignin with boron phosphate (BPO_4) groups. The disorder of the intermolecular H-bonding system during the oxidation process is thought for the gradual crystallinity loss together with the development of the amorphous phase for increased oxidation time.

The methine (CH) and methylene (CH_2) bands located at 2922, 2900, and 2860 cm^{-1} also lost most of their intensities, but a minor amount still remained, demonstrating that all H-species are not involved in dehydrogenation and dehydration processes. It is clear that the gradual loss of the H-bonded OH groups and H of the CH groups with growing oxidation time is a clear indication that dehydrogenation and dehydration processes took place in the oxidation process. Gradual reduction of intermolecular hydrogen bonding between OH groups of flax fibers using intensity ratios of (A_{3290}/A_{2900}) and (A_{3240}/A_{2900}) defined as hydrogen-bonding index (HBI) for different oxidation duration is presented quantitatively in Fig. 8. The infrared spectrum located at 2900 cm^{-1} was taken as an internal standard for normalization purposes [56]. The vibration located at 2900 cm^{-1} is clearly well-defined and prominent vibration in the pristine flax fiber. The use of the internal standard vibration makes it easy to make comparisons between different specimens for different oxidation duration.

The infrared spectra of the raw and oxidized flax fibers in the range 2000–400 cm^{-1} of raw and DAP-BAU incorporated-stabilized flax fibers for different oxidation periods are presented in Fig. 9. The wavenumber range 2000 to 400 cm^{-1} of the cellulose infrared spectra is known to be the most suitable portion for both quantitative and qualitative analysis. The physically absorbed water gives a

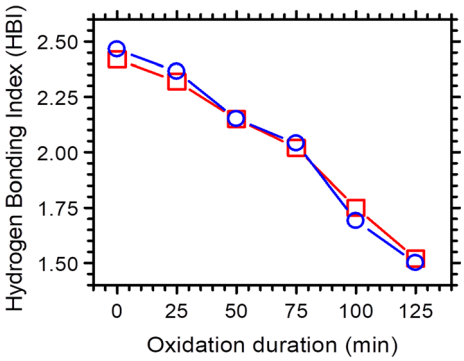

Figure 8 Changing of absorbance ratio (A_{3290}/A_{2900}) marked as (□), and (A_{3340}/A_{2900}) marked as (O) for variable oxidation durations. The absorbance value of 2900 cm^{-1} was considered as an internal standard.

distinctive spectrum at approximately 1640 cm^{-1}, while the infrared spectra of original flax fibers located around 1428, 1370, 1337, 1315, 1280, 1220, 1160, and 895 cm^{-1} are stated as delicate to crystallinity and lattice category [52].

Infrared spectra of pristine and oxidized flax fibers in the presence of DAP-BAU impregnation in the range 1850–1200 cm^{-1} for 25 min oxidation time are presented in Fig. 10. Carbonyl stretching vibration located at 1730 cm^{-1} allocated to C = O stretching band is moved to 1715 cm^{-1} indicating strong interaction with OH groups in forming H-bonds [58].

IR spectra in Fig. 9 indicate that the carbonyl (C = O) intensity grows with increasing oxidation time. This outcome strongly suggests that oxygen-containing functional groups are incorporated in the oxidation reactions. The ratio of the absorbance value of the carbonyl (C = O) band at 1715 to 2900 cm^{-1} is

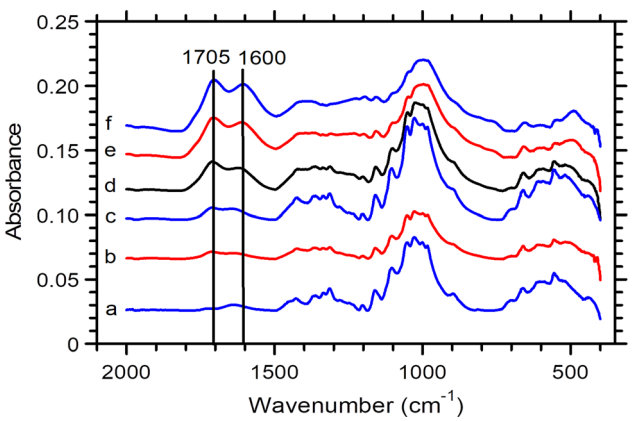

Figure 9 IR spectra in the range 2000–400 cm^{-1} of raw **a** and DAP-BAU pretreated-oxidized flax fibers for variable oxidation durations. **b** 25 min; **c** 50 min; **d** 75 min; **e** 100 min; **f** 125 min.

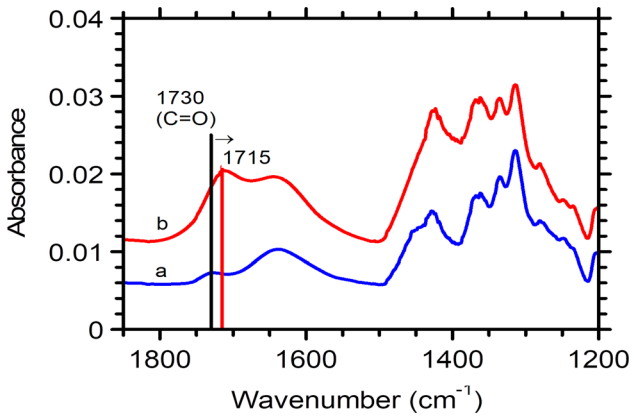

Figure 10 Infrared spectra of raw **a** and DAP-BAU pretreated-oxidized (25 min) flax fibers in the range 1850–1200 cm^{-1}.

defined as an oxidation index, where 2900 cm^{-1} is used here for comparison purposes. The results presented in Fig. 11 suggest that the oxidation index increases with increasing oxidation time suggesting increased oxygen content.

A completely new band at approximately 1610 cm^{-1} seemed like a strong vibration assigned to C = C stretching come to be prime in the samples oxidized at 25 min oxidation time and higher, suggesting the formation of the highly aromatic structure during the oxidation procedure. The infrared spectrum at 1610 cm^{-1} appeared as a shoulder in the IR spectrum obtained after the oxidation time of 25 min but became stronger with increasing oxidation time. The absorbance ratio of A_{1610}/A_{2900} is defined as the IR-aromatization index, and the values are presented in Fig. 12 that shows increasing aromatization index values with increasing oxidation time. The spectrum at 895 cm^{-1} allotted to asymmetrical out of phase cellulose ring stretching (C–O–C) lost intensity for the oxidation reactions with increasing oxidation time, indicating the replacement of hydrogen atoms from the cellulose, hemicellulose, and lignin structures by functional groups or owing to the creation of ring structures [52].

The IR spectrum located at 1370 cm^{-1} assigned to the CH_2 bending mode of crystalline cellulose is used for the evaluation of the degree of total crystallinity index (TCI) values using the intensity ratios of A_{1370}/A_{2900} for the pristine and oxidized flax samples [52]. The variation of the total crystallinity index is presented in Fig. 13 for variable oxidation duration. The outcomes demonstrate reduced crystallinity and increasing amorphous content for increased oxidation duration.

The IR spectroscopy was also used to assess the values of lateral index values using the absorbance ratios of A_{1430}/A_{895} as suggested in the published literature [52]. Figure 14 shows the changing values of the lateral order index for the pristine and oxidized flax samples as a function of oxidation time. The outcomes point to a continuous decrease in the values of lateral order index for the pristine and oxidized flax samples. It is clear that the values of the total crystallinity index are higher as expected than the lateral order index.

X-ray diffraction analysis (XRD)

Equatorial X-ray diffraction traces of pristine and thermally oxidized flax fibers are plotted in Fig. 15. Investigation of the equatorial XRD profile of raw flax

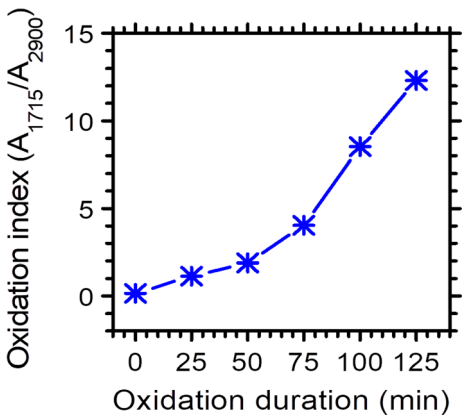

Figure 11 Changing of oxidation index (A_{1715}/A_{2900}) for variable oxidation durations.

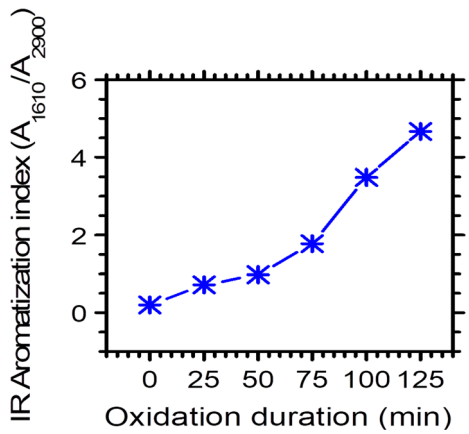

Figure 12 Changing of IR aromatization index (A_{1610}/A_{2900}) for variable oxidation durations.

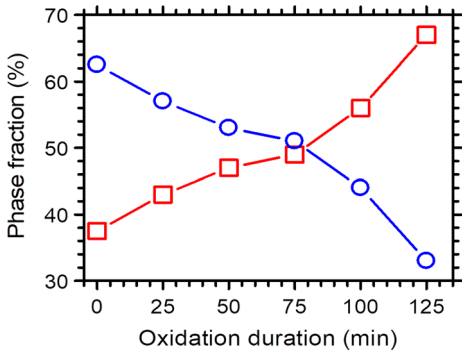

Figure 13 Comparison of infrared crystallinity and amorphous fraction of raw and DAP-BAU pretreated-oxidized flax fibers for variable oxidation durations. (O) crystalline phase, (□) amorphous phase.

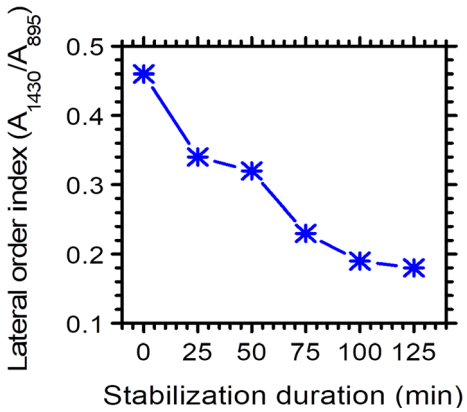

Figure 14 Lateral order index (LOI) values of raw and DAP-BAU pretreated-oxidized flax fibers for variable oxidation durations. (1430 cm^{-1} as a crystalline band and 895 cm^{-1} as a reference band).

fibers shows the availability of four distinct crystalline peaks as the most prominent reflections.

A curve-fitting technique has been utilized to acquire precise peak parameters for the equatorial X-ray diffraction profiles. Curve-fitting was used to evaluate amorphous ratio, apparent X-ray crystallinity, crystal size, and X-ray oxidation index for variable oxidation durations. The equatorial XRD profile of flax fibers presented in Fig. 16 can be determined from five crystalline peaks of cellulose I structure located at about 14.7 ± 0.3, 16.4 ± 0.3, 21.4 ± 0.2, 22.4 ± 0.2, and 34.8 ± 0.3 attributed to (101), (10 $\bar{1}$), (120/200), (002), and (040) reflections. These bands relate to a monoclinic unit cell. It is obvious that the 002 peak intensity is the sturdiest comparing with (101), (10 $\bar{1}$), (120/200), and (040) peak intensities. The peak parameters acquired from

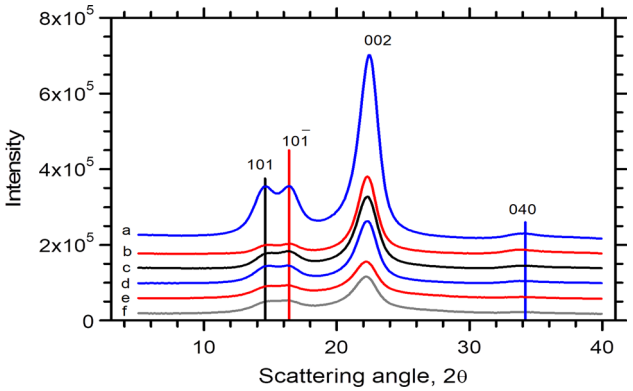

Figure 15 Equatorial X-ray diffraction profiles of raw **a** and DAP-BAU pretreated-oxidized flax fibers for variable oxidation durations. **b** 25 min; **c** 50 min; **d** 75 min; **e** 100 min; **f** 125 min.

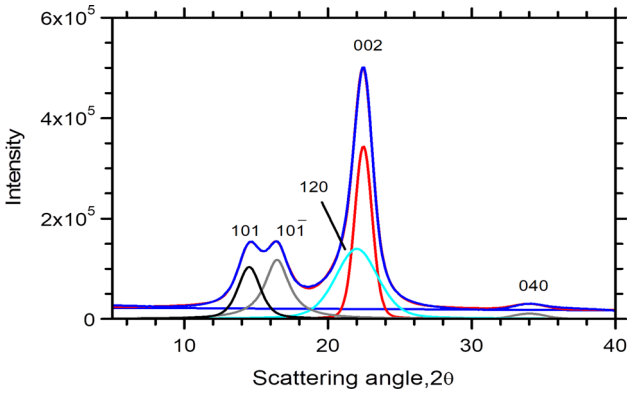

Figure 16 Curve-fitting of equatorial X-ray diffraction trace of raw flax fiber.

the curve-fitting technique of raw flax fibers are presented in Table 3, along with the comparative assessment of the calculated and observed d-spacing values.

DAP-BAU incorporation followed by oxidation in the air atmosphere at 245 °C and oxidation times ranging from 25 to 125 min showed an impressive influence on the crystalline structure of flax fiber as

Table 3 Resolved peak parameters of curve-fitted XRD trace of raw flax fiber

Hkl	F	A	W	*P* (2θ)	d_{obs} (nm)	d_{calc} (nm)
101	0.47	103,580	1.85	14.75	0.600	0.603
10 $\bar{1}$	0.99	118,047	2.04	16.35	0.542	0.543
120/200	0.29	139,975	3.47	21.43	0.414	0.415
002	0.13	343,929	1.43	22.55	0.394	0.392
040	0.00	10,576	2.62	34.4	0.260	0.258

the degree of apparent crystallinity of the cellulose I structure. A close investigation of the XRD profiles presented in Fig. 15 exhibited a steady loss of crystal structure for higher oxidation times. The loss of the intensity of the XRD profiles indicates the development of amorphization (i.e., decrystallization) reactions with growing oxidation time. The findings presented in Table 4 demonstrate that all of the crystalline peaks seem to survive with progressing oxidation reactions due to ongoing oxidation reactions through the oxidation time from 25 to 125 min.

Curve-fitting of XRD profile of 50 min oxidized flax fiber is presented in Fig. 17. Peak areas acquired from the curve-fitting of XRD traces were utilized to assess the ratios of amorphous and crystalline (i.e., cellulose *I*) structures employing Eq. 1. The findings presented in Fig. 18 indicate that the X-ray crystallinity was reduced from 68.8 to 38.9% after 125 min oxidation duration. In contrast, the amorphous fraction increased from 31.2 to 61.1% after the oxidation time of 125 min.

X-ray oxidation index was evaluated employing the intensity of the (002) as a prominent reflection by using Eq. 2. The outcomes showed in Fig. 19 illustrate the X-ray oxidation indices for the oxidized flax samples for variable oxidation durations. With increasing oxidation duration from 25 to 125 min, the X-ray oxidation index was increased from 0 to 88%. Evaluation X-ray oxidation index is considered as a dependable way in assessing the fraction of aromatic and crosslinked structures formed in the course of oxidation reactions [37]. The experimental outcomes point out that DAP-BAU impregnated and oxidized flax fibers in an air atmosphere resulted in the gradual disappearance of cellulose I crystal structure and a rise in the disordered fraction along with the

Table 4 The presence and absence of X-ray diffraction reflections of raw and DAP-BAU pretreated-oxidized flax fibers

Stabilization duration (min)	101	10 $\bar{1}$	002	040
0	+	+	+	+
25	+	+	+	+
50	+	+	+	+
75	+	+	+	+
100	+	+	+	+
125	+	+	+	+

(+) Reflection is present

(−) Reflection is absent

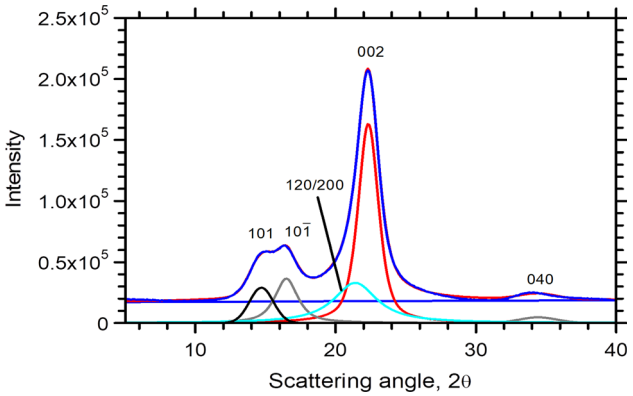

Figure 17 Curve-fitting of equatorial XRD trace of 50 min thermally stabilized flax fiber.

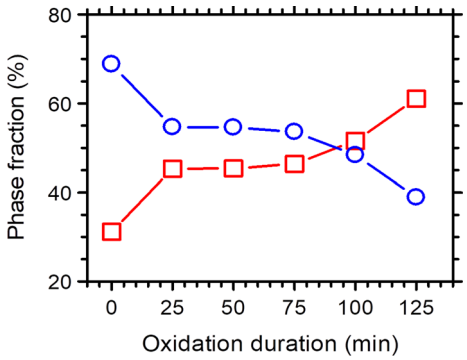

Figure 18 Comparison X-ray crystallinity and amorphous fraction of raw and oxidized flax fibers for variable oxidation durations. (O) crystalline phase; (□) amorphous phase.

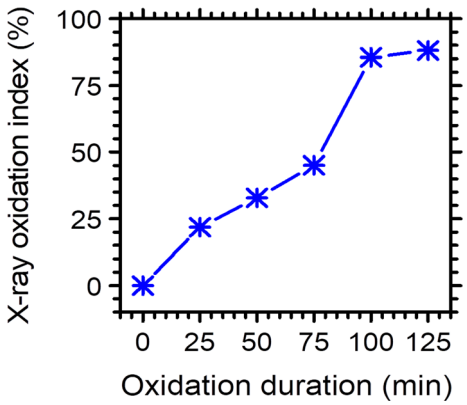

Figure 19 Comparison of X-ray oxidation index of raw and oxidized flax fibers for variable oxidation durations.

improvement in the ratio of the cyclized structure comprising crosslinked ladder-like structural units.

During the oxidation reactions, 101, 10 $\bar{1}$, 120/200, and 040 reflections kept their presence during the oxidation reactions. The most prominent (002) peak

also kept its presence during the oxidations reactions. The half-height widths of the reflections broadened with growing oxidation times, indicating the progressive reduction in the crystal dimensions. This result comes as a result of the breaking up structure in the decrystallization reactions [37]. The gradual intensity decrease of the 101, 10 $\bar{1}$, 120/200, 002, and 040 peaks is supposed as a result of breaking the cellulose I crystal structure due to the ongoing decrystallization reactions.

Since the (002) reflection kept its presence during the oxidation process, it was used for the evaluation of crystal size during the oxidation process. Evaluation of crystal sizes of the raw and oxidized flax fibers was performed using Eq. 3. Figure 20 shows the values of corrected crystal size corresponding to prominent (002) peak as a function of oxidation time. Crystal size for (002) reflection was reduced from 6.6 to 3.6 nm with growing oxidation durations due to the ongoing decrystallization process.

Conclusions

DAP-BAU aqueous solution impregnation and multistep thermal oxidation of flax fiber were performed in the air atmosphere at temperatures up to 245 °C. The investigation of DSC profiles showed that DAP-BAU pretreatment enhanced thermal stability by inhibiting the fundamental hydroxyl groups and restricted the development of volatile by-products. In the initial stages of oxidation, the DSC traces revealed a notable decrease in the decomposing temperature and then slowed decomposition reactions in the following steps. TGA thermograms have demonstrated an improvement in thermal stability, as seen by increased char yield with increasing oxidization times. The findings of the XRD investigation indicated that the crystalline structure had been lost and that the original cellulose structures had been converted to a strongly cyclized and crosslinked structure at increased oxidation duration. Intermolecular and intramolecular H-bonds and methine (CH) bands related to hydrogenation and dehydration reactions were shown to have a steady decrease of intensity of OH stretching in the infrared spectroscopy analysis. In the wavenumber range between 1900 and 800 cm^{-1}, IR data analysis indicated the interference of the crystalline structure for higher oxidation duration confirms the findings of X-ray diffraction analyses.

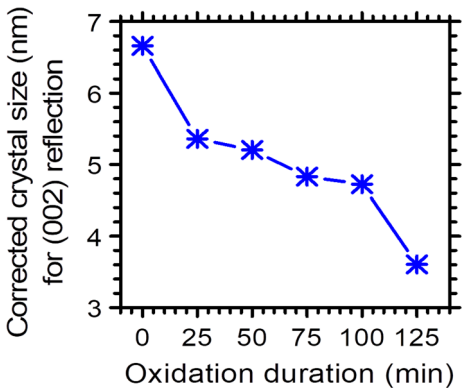

Figure 20 Comparison of the crystal size for (002) peak of raw and oxidized flax fibers for variable oxidation durations.

Acknowledgements

This study was supported by a grant from the Higher Education Council of Turkey to Md. Mahbubor Rahman under the YÖK Scholarship Program.

Declarations

Conflict of interest There are no conflicts of interest among the authors.

References

[1] Zhang S, Shao T, Kose HS, Karanfil T (2010) Adsorption of aromatic compounds by carbonaceous adsorbents: a comparative study on granular activated carbon, activated carbon fiber, and carbon nanotubes. Environ Sci Technol 44:6377–6383. https://doi.org/10.1021/es100874y

[2] Subramanian V, Luo C, Stephan AM et al (2007) Supercapacitors from activated carbon derived from banana fibers. J Phys Chem C 111:7527–7531. https://doi.org/10.1021/jp067009t

[3] Nandi M, Okada K, Dutta A et al (2012) Unprecedented CO 2 uptake over highly porous N-doped activated carbon monoliths prepared by physical activation. Chem Commun 48:10283–10285. https://doi.org/10.1039/C2CC35334B

[4] Pelekani C, Snoeyink VL (1999) Competitive adsorption in natural water: role of activated carbon pore size. Water Res 33:1209–1219. https://doi.org/10.1016/S0043-1354(98)00329-7

[5] Alcañiz-Monge J, Linares-Solano A, Rand B (2002) Mechanism of adsorption of water in carbon micropores as

revealed by a study of activated carbon fibers. J Phys Chem B 106:3209–3216. https://doi.org/10.1021/jp014388b

[6] Cabiac A, Cacciaguerra T, Trens P et al (2008) Influence of textural properties of activated carbons on Pd/carbon catalysts synthesis for cinnamaldehyde hydrogenation. Appl Catal A Gen 340:229–235. https://doi.org/10.1016/j.apcata.2008.02.018

[7] Caqueret V, Bostyn S, Cagnon B, Fauduet H (2008) Purification of sugar beet vinasse–adsorption of polyphenolic and dark colored compounds on different commercial activated carbons. Bioresour Technol 99:5814–5821. https://doi.org/10.1016/j.biortech.2007.10.009

[8] Horikawa T, Hayashi J, Muroyama K (2002) Preparation of molecular sieving carbon from waste resin by chemical vapor deposition. Carbon N Y 40:709–714. https://doi.org/10.1016/S0008-6223(01)00157-9

[9] Khomenko V, Raymundo-Piñero E, Béguin F (2008) High-energy density graphite/AC capacitor in organic electrolyte. J Power Sources 177:643–651. https://doi.org/10.1016/j.jpowsour.2007.11.101

[10] Rosas JM, Bedia J, Rodríguez-Mirasol J, Cordero T (2009) HEMP-derived activated carbon fibers by chemical activation with phosphoric acid. Fuel 88:19–26. https://doi.org/10.1016/j.fuel.2008.08.004

[11] Williams PT, Reed AR (2006) Development of activated carbon pore structure via physical and chemical activation of biomass fibre waste. Biomass Bioenerg 30:144–152. https://doi.org/10.1016/j.biombioe.2005.11.006

[12] Fu R, Liu L, Huang W, Sun P (2003) Studies on the structure of activated carbon fibers activated by phosphoric acid. J Appl Polym Sci 87:2253–2261. https://doi.org/10.1002/app.11607

[13] Zeng F, Pan D, Pan N (2005) Choosing the impregnants by thermogravimetric analysis for preparing rayon-based carbon fibers. J Inorg Organomet Polym Mater 15:261–267. https://doi.org/10.1007/s10904-005-5543-3

[14] Zhang Z, Li J, Sun F et al (2011) Preparation and characterization of activated carbon fiber from paper. Chinese J Chem Phys 24:103–108. https://doi.org/10.1088/1674-0068/24/01/103-108

[15] Uraki Y, Nakatani A, Kubo S, Sano Y (2001) Preparation of activated carbon fibers with large specific surface area from softwood acetic acid lignin. J Wood Sci 47:465–469. https://doi.org/10.1007/BF00767899

[16] Asakura R, Morita M, Maruyama K et al (2004) Preparation of fibrous activated carbons from wood fiber. J Mater Sci 39:201–206. https://doi.org/10.1023/B:JMSC.0000007745.62879.74

[17] Phan NH, Rio S, Faur C et al (2006) Production of fibrous activated carbons from natural cellulose (jute, coconut) fibers for water treatment applications. Carbon N Y 44:2569–2577. https://doi.org/10.1016/j.carbon.2006.05.048

[18] Li K, Li Y, Hu H (2011) Adsorption characteristics of lead on cotton-stalk-derived activated carbon fibre by steam activation. Desalin Water Treat 30:1–9. https://doi.org/10.5004/dwt.2011.1130

[19] Jimenez V, Sánchez P, Romero A (2017) Materials for activated carbon fiber synthesis. Activated carbon fiber and textiles. Elsevier, Amsterdam, pp 21–38

[20] He D, Wu L, Yao Y et al (2020) A facile route to high nitrogen-containing porous carbon fiber sheets from biomass-flax for high-performance flexible supercapacitors. Appl Surf Sci 507:145108. https://doi.org/10.1016/j.apsusc.2019.145108

[21] Aliotta L, Gigante V, Coltelli M-B et al (2019) Thermo-mechanical properties of PLA/short flax fiber biocomposites. Appl Sci 9:3797. https://doi.org/10.3390/app9183797

[22] Dumanlı AG, Windle AH (2012) Carbon fibres from cellulosic precursors: a review. J Mater Sci 47:4236–4250. https://doi.org/10.1007/s10853-011-6081-8

[23] Il KM, Park M-S, Lee Y-S (2016) Cellulose-based carbon fibers prepared using electron-beam stabilization. Carbon Lett 18:56–61. https://doi.org/10.5714/CL.2016.18.056

[24] Fukuzumi H, Saito T, Okita Y, Isogai A (2010) Thermal stabilization of TEMPO-oxidized cellulose. Polym Degrad Stab 95:1502–1508. https://doi.org/10.1016/j.polymdegradstab.2010.06.015

[25] Bengtsson A, Bengtsson J, Sedin M, Sjöholm E (2019) Carbon fibers from lignin-cellulose precursors: effect of stabilization conditions. ACS Sustain Chem Eng 7:8440–8448. https://doi.org/10.1021/acssuschemeng.9b00108

[26] Byrne N, De Silva R, Ma Y et al (2018) Enhanced stabilization of cellulose-lignin hybrid filaments for carbon fiber production. Cellulose 25:723–733. https://doi.org/10.1007/s10570-017-1579-0

[27] Gregorová A, Košíková B, Moravčík R (2006) Stabilization effect of lignin in natural rubber. Polym Degrad Stab 91:229–233. https://doi.org/10.1016/j.polymdegradstab.2005.05.009

[28] Yue Z, Vakili A, Hosseinaei O, Harper DP (2017) Lignin-based carbon fibers: Accelerated stabilization of lignin fibers in the presence of hydrogen chloride. J Appl Polym Sci 134:45507. https://doi.org/10.1002/app.45507

[29] Kadla JF, Kubo S, Gilbert RD, Venditti RA (2002) Lignin-Based Carbon Fibers BT - Chemical Modification, Properties, and Usage of Lignin. In: Hu TQ (ed). Springer US, Boston, MA, pp 121–137

[30] Akpan EI (2019) Stabilization of Lignin Fibers BT - Sustainable Lignin for Carbon Fibers: Principles, Techniques,

and Applications. In: Akpan EI, Adeosun SO (eds). Springer International Publishing, Cham, pp 325–352

[31] Nam S, Condon BD, Parikh DV et al (2011) Effect of urea additive on the thermal decomposition of greige cotton nonwoven fabric treated with diammonium phosphate. Polym Degrad Stab 96:2010–2018. https://doi.org/10.1016/j.polymdegradstab.2011.08.014

[32] Nuessle AC, Ford FM, Hall WP, Lippert AL (1956) Some aspects of the cellulose-phosphate-urea reaction. Text Res J 26:32–39. https://doi.org/10.1177/004051755602600105

[33] Blanchard EJ, Graves EE (2003) Phosphorylation of cellulose with some phosphonic acid derivatives. Text Res J 73:22–26. https://doi.org/10.1177/004051750307300104

[34] Chau CN, Smith JA (1992) Method of making luminescent grade boron phosphate. US Patent 5082640

[35] Gaan S, Sun G (2007) Effect of phosphorus and nitrogen on flame retardant cellulose: a study of phosphorus compounds. J Anal Appl Pyrolysis 78:371–377. https://doi.org/10.1016/j.jaap.2006.09.010

[36] Karacan I, Baysal G (2012) Investigation of the effect of cupric chloride on thermal stabilization of polyamide 6 as carbon fiber precursor. Fibers Polym 13:864–873. https://doi.org/10.1007/s12221-012-0864-7

[37] Karacan I, Soy T (2013) Enhancement of oxidative stabilization of viscose rayon fibers impregnated with ammonium sulfate prior to carbonization and activation steps. J Appl Polym Sci 128:1239–1249. https://doi.org/10.1002/app.38496

[38] Rahman MM, Demirel T, Tunçel KŞ, Karacan I (2021) The effect of the ammonium persulfate and a multi-step annealing approach during thermal stabilization of polyacrylonitrile multifilament prior to carbonization. J Mater Sci 56:14844–14865. https://doi.org/10.1007/s10853-021-06209-1

[39] Hindeleh AM, Johnson DJ, Montague PE (1980) Computational methods for profile resolution and crystallite size evaluation in fibrous polymers. ACS Publications, Washington, DC, pp 149–182

[40] Hindeleh AM, Johnson DJ (1978) Crystallinity and crystallite size measurement in polyamide and polyester fibres. Polymer (Guildf) 19:27–32. https://doi.org/10.1016/0032-3861(78)90167-2

[41] Yu M-J, Bai Y-J, Wang C-G et al (2007) A new method for the evaluation of stabilization index of polyacrylonitrile fibers. Mater Lett 61:2292–2294. https://doi.org/10.1016/j.matlet.2006.08.071

[42] Stokes AR (1948) A numerical Fourier-analysis method for the correction of widths and shapes of lines on X-ray powder photographs. Proc Phys Soc 61:382–391. https://doi.org/10.1088/0959-5309/61/4/311

[43] Arseneau DF (1971) Competitive reactions in the thermal decomposition of cellulose. Can J Chem 49:632–638. https://doi.org/10.1139/v71-101

[44] Shafizadeh F, Bradbury AGW (1979) Thermal degradation of cellulose in air and nitrogen at low temperatures. J Appl Polym Sci 23:1431–1442. https://doi.org/10.1002/app.1979.070230513

[45] Mwaikambo LY, Ansell MP (2002) Chemical modification of hemp, sisal, jute, and kapok fibers by alkalization. J Appl Polym Sci 84:2222–2234. https://doi.org/10.1002/app.10460

[46] Kabir MM, Islam MM, Wang H (2013) Mechanical and thermal properties of jute fibre reinforced composites. J Multifunct Compos 1:71–77. https://doi.org/10.12783/issn.2168-4286/1.1/Islam

[47] Sharma HSS, van Sumere CF (1992) The Biology and processing of flax. M Publications, Belfast

[48] Thuault A, Eve S, Blond D et al (2014) Effects of the hygrothermal environment on the mechanical properties of flax fibres. J Compos Mater 48:1699–1707. https://doi.org/10.1177/0021998313490217

[49] Kondo T (1997) The assignment of IR absorption bands due to free hydroxyl groups in cellulose. Cellulose 4:281–292. https://doi.org/10.1023/A:1018448109214

[50] Khan MA, Hassan MM, Drzal LT (2005) Effect of 2-hydroxyethyl methacrylate (HEMA) on the mechanical and thermal properties of jute-polycarbonate composite. Compos Part A Appl Sci Manuf 36:71–81. https://doi.org/10.1016/j.compositesa.2004.06.027

[51] Tsuboi M (1957) Infrared spectrum and crystal structure of cellulose. J Polym Sci 25:159–171. https://doi.org/10.1002/pol.1957.1202510904

[52] Carrillo F, Colom X, Valldeperas J et al (2003) Structural characterization and properties of lyocell fibers after fibrillation and enzymatic defibrillation finishing treatments. Text Res J 73:1024–1030. https://doi.org/10.1177/004051750307301114

[53] Fanti G, Baraldi P, Basso R, Tinti A (2013) Non-destructive dating of ancient flax textiles by means of vibrational spectroscopy. Vib Spectrosc 67:61–70. https://doi.org/10.1016/j.vibspec.2013.04.001

[54] Nelson ML, O'Connor RT (1964) Relation of certain infrared bands to cellulose crystallinity and crystal lattice type. Part II. A new infrared ratio for estimation of crystallinity in celluloses I and II. J Appl Polym Sci 8:1325–1341. https://doi.org/10.1002/app.1964.070080323

[55] Liang CY, Marchessault RH (1959) Infrared spectra of crystalline polysaccharides. I. Hydrogen bonds in native celluloses. J Polym Sci 37:385–395. https://doi.org/10.1002/pol.1959.1203713209

[56] Roy A, Chakraborty S, Kundu SP et al (2012) Improvement in mechanical properties of jute fibres through mild alkali treatment as demonstrated by utilisation of the Weibull distribution model. Bioresour Technol 107:222–228. https://doi.org/10.1016/j.biortech.2011.11.073

[57] Dadashian F, Yaghoobi Z, Wilding MA (2005) Thermal behaviour of lyocell fibres. Polym Test 24:969–977. https://doi.org/10.1016/j.polymertesting.2005.08.005

[58] Abdelmouleh M, Boufi S, Belgacem MN et al (2004) Modification of cellulosic fibres with functionalised silanes: development of surface properties. Int J Adhes Adhes 24:43–54. https://doi.org/10.1016/S0143-7496(03)00099-X